Lagrangian chaos and correlated Lévy flights in a non-Beltrami flow: transient versus long-term transport

M.A. Fogleman†, M.J. Fawcett, and T. H. Solomon*
Department of Physics, Bucknell University, Lewisburg, PA 17837
(October 12, 2000)

Long-range transport is studied numerically in a time-independent, three-dimensional (3D) fluid flow composed of the superposition of two chains of alternating vortices, one horizontal and the other vertical. Tracers in this flow follow chaotic trajectories composed of correlated Lévy flights with varying velocities. Locations of the chaotic regimes in the flow are compared with recent theories of chaos in non-Beltrami 3D flows. Growth of the variance of a distribution of tracers is divided into transient and long-term regimes, each with different growth exponents.

05.40.Fb, 47.52.+j, 94.10.Lf, 05.45.Pq

It is well known that a simple, ordered fluid flow can have particle trajectories that are *chaotic* in the sense that nearby trajectories separate exponentially in time. [1] For a three-dimensional (3D) flow, chaotic trajectories are possible even if the flow is *time independent*, as was first explained by Arnol'd in 1965. [2] Arnol'd's theory, however, applies only to inviscid flows that satisfy the Beltrami condition $\vec{\nabla} \times \vec{u} = \lambda \vec{u}$, where $\vec{u}$ is the velocity field and λ is a constant. The theory of Lagrangian chaos in time-independent, 3D flows has been extended recently to include flows that are not inviscid and that do not satisfy the Beltrami condition. [3] This recent theory proposes that for a wide range of 3D, time-independent flows, Lagrangian chaos will be most commonly observed in regions of the flow where the diagnostic $|\vec{\nabla} \times \vec{\omega}|^2$ is largest.

Lagrangian chaos leads to significant enhancements in long-range transport. The long-term behavior of the transport has been studied extensively; specifically, in the long-time limit, the variance of a distribution of tracers typically grows as a power law: $\langle r^2 \rangle \sim t^\gamma$. According to the Central Limit Theorem, transport for $t \to \infty$ will be normally diffusive ($\gamma = 1$) if there are finite length and time scales to the motions of the tracers. On the other hand, superdiffusive ($\gamma > 1$) transport is possible if the trajectories are characterized by *Lévy flights* – long distance "jumps " (between regions with relatively little motion) with a wide range of lengths and durations and no finite scale. [4] Theories relating the flight statistics to long-term transport assume that flights are independent of each other (i.e., no correlations); furthermore, the short-time (transient) behavior of the transport is often neglected.

In this Rapid Communication, we present results of a numerical study of Lagrangian chaos and its effects on transient and long-term transport in a novel 3D, time-independent, non-Beltrami fluid flow. This flow is ideal for these studies due both to its simplicity and to its rich transport properties. Simulations of motion in the flow reveal Lévy flights and superdiffusive long-range transport. Furthermore, the growth of the variance is typically described by two different values of γ for different time regimes. The transient behavior is likely to be of significant importance for real systems, where issues of practical importance may occur over time scales far short of those needed to achieve the long-time limit common in theories of anomalous diffusion. We propose that this short-time behavior can be explained by considering correlations between flights, which result in clusters that must be considered when relating flight statistics to long-range transport.

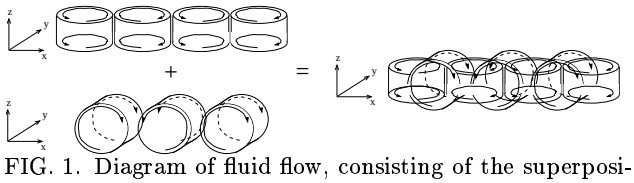

FIG. 1. Diagram of fluid flow, consisting of the superposition of a horizontal chain of alternating vortices with a vertical chain of alternating vortices.

The flow studied is the superposition of two chains of alternating vortices (Fig. 1). The equations describing the velocity field are

$$\begin{aligned} \dot{x} &= -a\tfrac{\lambda}{2d} cos(\tfrac{2\pi(x+0.5)}{\lambda}) sin(\tfrac{\pi y}{d}) - a_2 \tfrac{\lambda}{2d_2} cos(\tfrac{2\pi x}{\lambda}) sin(\tfrac{\pi z}{d_2}), \\ \dot{y} &= a sin(\tfrac{2\pi(x+0.5)}{\lambda}) cos(\tfrac{\pi y}{d}), \\ \dot{z} &= a_2 sin(\tfrac{2\pi x}{\lambda}) cos(\tfrac{\pi z}{d_2}). \end{aligned} \tag{1}$$

In these equations, a and a_2 are the magnitudes of the two superposed vortex chains, and d and d_2 are the width and height (respectively) of the fluid layer. Throughout the rest of the paper, all of the vortices are assumed to have unity aspect ratio: $d = d_2 = 1$ and $\lambda = 2$. Consequently, the variables x, y and z are all scaled by the vortex width/height. Furthermore, times are scaled by a characteristic advective time d/a. The relative magnitude of the two vortex chains is denoted by the amplitude ratio a/a_2.

Particle trajectories are determined numerically by integrating Eqs. 1 using a fourth-order Runge-Kutta technique. The results are shown in Figs. 2 and 3 for $a/a_2 = 5.0$ and 1.0, respectively.

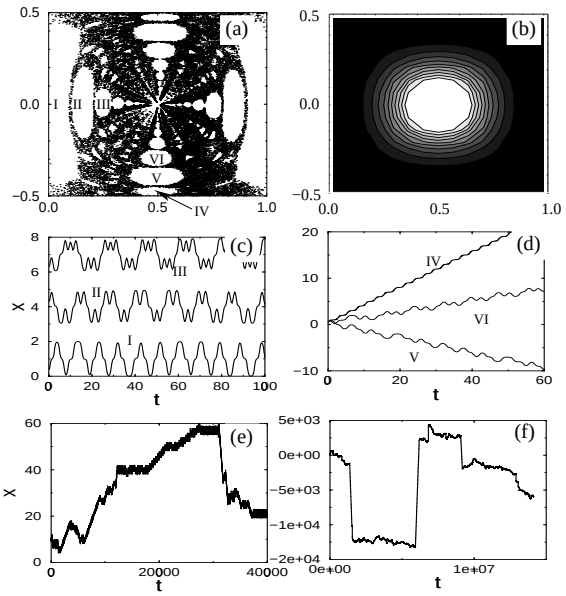

FIG. 2. Results of simulations for $a/a_2 = 5.0$. (a) Poincaré section at $z = 0.0$. (b) Diagnostic $|\vec{\nabla} \times \vec{\omega}|^2$. The white regions correspond to large values of $|\vec{\nabla} \times \vec{\omega}|^2$, where the theory predicts chaotic regions. (c) Sample trapped trajectories from ordered regions. Each curve is labelled with a roman numeral corresponding to an island in Fig. (a). (d) Sample untrapped trajectories from ordered regions. The differing velocities is apparent from the slopes of these curves. (e) and (f) Sample trajectories from chaotic region.

Poincaré sections are plotted in Figs. 2(a) and 3(a). The points in these plots show the x-y coordinates of a single tracer each time it passes through the mid-height ($z = 0$) of the system. Periodic boundary conditions have been used at the left and right. A single tracer in the chaotic region visits the entire region, resulting in an intricate stochastic web for both amplitude ratios with empty "islands" corresponding to regions containing ordered trajectories. Figures 2(b) and 3(b) show the diagnostic proposed by Yannacopoulos et al., [3] as applied to the flow in Eq. (1). It is apparent from the comparison between Figs. (a) and (b) in both cases that the diagnostic works quite well at identifying regions where Lagrangian chaos is most likely to be found.

The x-coordinate of the particle trajectories (plotted in Fig. 2(c) - (f) for $a/a_2 = 5.0$) is the one most relevant to discussions of long-range transport. Figures 2(c) and (d) show ordered trajectories for tracers confined to the appropriately-labelled islands in Fig. 2(a). The oscillatory behavior is due to figure-8 motion between adjacent horizontal vortices, with increasing number of loops for islands near the centers for $a/a_2 = 5.0$.

Of particular importance are the unbounded trajectories, such as those plotted in Fig. 2(d). Tracers undergoing these trajectories snake their way around and between the vortices, traveling very long distances (at least several times longer than a vortex width) in short periods of time, with the average x-velocity determined by the number of loops executed in each vortex before crossing to the next. Tracers in the stochastic region (Fig. 2(e) and (f)) temporarily stick to the outsides of the islands, [5] mimicking the behavior of the corresponding ordered trajectory while stuck. The sticking process results in flights with a wide range of lengths and durations for the chaotic trajectories. It is striking that flights of these lengths are possible in this flow, even though there are no jet regions. Several different flight velocities are possible, depending on which island the tracer is sticking during the flights. Similar behavior is observed for $a/a_2 = 1.0$ (Fig. 3(c) and (d)), although trapping is not as significant as for the case with $a/a_2 = 5.0$.

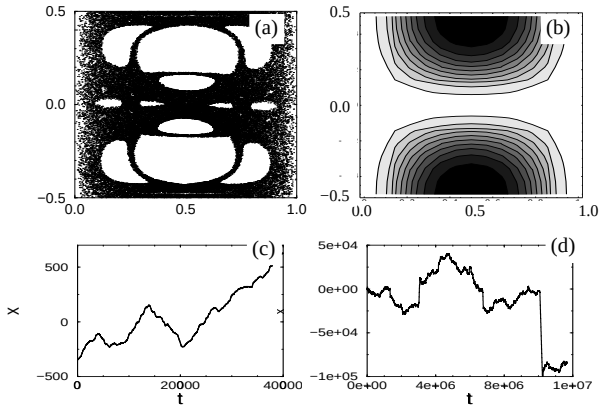

FIG. 3. Results of simulations for $a/a_2 = 1.0$. (a) Poincaré section at $z = 0.0$. (b) Diagnostic $|\vec{\nabla} \times \vec{\omega}|^2$. The white regions correspond to large values of $|\vec{\nabla} \times \vec{\omega}|^2$, where the theory predicts chaotic regions. (c) and (d) Sample trajectories from chaotic region.

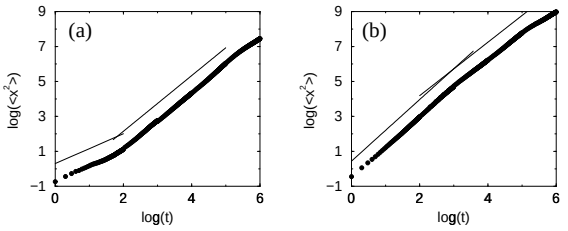

FIG. 4. Growth of the variance of a distribution. Fits (thin solid lines) show the scaling regions; all fits are raised by 1 unit to distinguish from the data. (a) Amplitude ratio $a/a_2 = 5.0$; slope is 0.85 ± 0.20 from log(t) = 0 to 1.5 and is 1.6 ± 0.2 from log(t) = 2.0 to 4.6. (b) $a/a_2 = 1.0$; slope is 1.8 ± 0.2 from log(t) = 1.0 to 3.2 and 1.5 ± 0.2 from log(t) = 3.2 to 5.2.

The variance of a spreading ensemble of tracers is plotted in Figs. 4(a) and (b) for amplitude ratios 5.0 and 1.0, respectively. In both cases, there is a transient regime followed by a longer-term regime. For $a/a_2 = 5.0$ (Fig. (a)), the transient behavior is approximately diffusive ($\gamma = 0.85 \pm 0.20$), while the long-term behavior is su-

perdiffusive ($\gamma = 1.6 \pm 0.2$). For $a/a_2 = 1.0$ (Fig. (b)), the transient behavior is almost ballistic ($\gamma = 1.8 \pm 0.2$), followed by a superdiffusive regime with $\gamma = 1.5 \pm 0.2$.

To explain the transport behavior shown in Fig. 4, it is necessary to determine the statistics of the flights and trapping events. Theories [6] have been developed that demonstrate that superdiffusion can occur if a tracer undergoes flights whose lengths have diverging second moment: $\langle L^2 \rangle \to \infty$. This condition – which defines Lévy flights – is met if the probability distribution function (PDF) for flight lengths has a power law tail $p(L) \sim L^{-\mu}$ with $\mu < 3$. If the *trapping time* PDF has a *finite* second moment and if the flights all have the same constant speed, then the variance is predicted [6] to grow as

$$\gamma = \left\{ \begin{array}{l} 2, \mu < 2 \\ 4 - \mu, 2 < \mu < 3 \\ 1, \mu > 3 \end{array} \right\} \qquad (2)$$

Since there are no jet regions in this flow, a tracer meanders around and between the vortices during a flight. The fastest flights correspond to tracers that enter a vortex at one corner, circle half-way around, and exit at the opposite corner. The result is a snake-like trajectory. For the smaller velocity flights, the tracer undergoes an integral number of additional rotations within each horizontal vortex before continuing on to the next vortex. Identification of flights is facilitated by plotting the x- and t- coordinates only when the tracer crosses the center of a horizontal vortex, i.e., when it crosses $x = 0.0, 1.0, 2.0, \ldots$. The fastest flights will be revealed as a continually increasing (or decreasing) sequence of vortex centers; e.g., $x = 2, 3, 4, 5, 6, \ldots$. The next fastest flights will have an extra loop in each vortex, which shows up as two additional crossings of each vortex center; e.g., $x = 2, 3, 3, 3, 4, 4, 4, 5, 5, 5, \ldots$. Each flight is associated with a direction and a speed, which is characterized by the number of repeats of each vortex center crossing. A flight is considered to have ended if either (a) the direction of motion changes; or (b) the number of repeats per vortex changes.

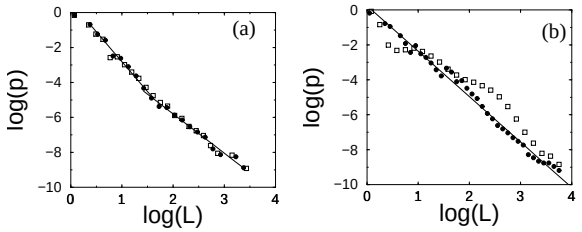

FIG. 5. Probability distribution functions (PDFs) for flights. The filled circles show PDFs for individual flights, while the open squares correspond to the PDF of lengths of flight clusters. (a) $a/a_2 = 5.0$; fitted slope is -3.4 ± 0.2 for $0.4 < log(t) < 1.6$ and is -2.3 ± 0.2 for $1.4 < log(t) < 3.4$. (b) $a/a_2 = 1.0$; fitted slope is -2.6 ± 0.2.

Logarithmic plots of the PDFs for flight length are shown in Fig. 5 (filled circles). The PDFs for both amplitude ratios have algebraic tails with decay exponents consistent with the definition of a Lévy flight: $\mu = 2.3$ and 2.6 ± 0.2 for $a/a_2 = 5.0$ and 1.0, respectively. Trapping duration PDFs (not shown) also have algebraic tails, but with exponents $\nu = 3.5$ and 4.2 (± 0.2) for amplitude ratios of 5.0 and 1.0, respectively. These exponents are both greater than 3; consequently, the trapping time PDFs have finite second moment, and the prediction in Eq. 2 should hold. Comparing the flight exponents μ from Fig. 5 and the superdiffusive exponents γ from Fig. 4, we find that the long-time behavior is consistent with the predictions from Eq. 2.

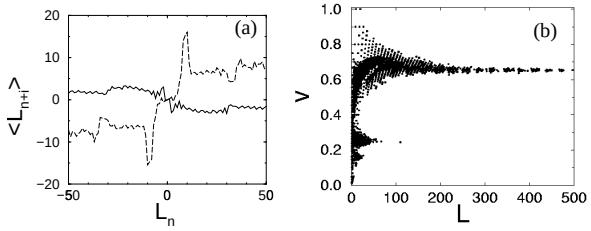

FIG. 6. Supporting data for $a/a_2 = 1.0$. (a) Correlations between flights; average length for next flight (n+1 – solid line) and for following flight (n+2 – dashed line). The data shows that a medium-to-long flight is likely to be followed by another long flight in the same direction after a small motion backward. (b) Scatter plot of flight length L and speed v. The lower speed flights decay away for smaller lengths than those with $v = 0.65$.

The transient behavior for $a/a_2 = 5.0$ can be explained from the framework of Eq. 2. Smaller length flights for this amplitude ratio have a larger decay exponent; $\mu = 3.4 \pm 0.2$, as seen in Fig. 5(a). Since $\mu > 3$ for the small length flights, the PDF is not consistent with Lévy scaling for small lengths (and, consequently, transient times), so the transport should be diffusive over small timescales. This is consistent with the transient growth exponent $\gamma = 0.85 \pm 0.20$ in Fig. 4(a).

For $a/a_2 = 1.0$, however, there is no kink in the PDF for flight lengths (filled circles in Fig. 5(b)). To explain the almost ballistic transport at short times in Fig. 4(b) it is necessary to consider the fact that the flights are not independent. In fact, there are significant correlations between a flight and the subsequent two flights, as shown in Fig. 6a for $a/a_2 = 1.0$. As shown by the solid curve in this figure, a flight of length L_n in a particular direction is followed – on the average – by a flight with a small average length $\langle L_{n+1} \rangle$ in the opposite direction. The dashed curve, however, shows that the *next* flight (the second one after the original forward flight) on the average returns back (and beyond) in the original direction by an average $\langle L_{n+2} \rangle$ of 10 vortex widths in the initial direction.

Because of these correlations, flights tend to form clusters with overall lengths that are frequently *significantly*

longer than individual flights. Clusters are determined by the following algorithm: given a flight with a particular direction, if the next two flights add up to produce a total jump of three or more vortex widths in the same direction, then those two flights are combined with the first to form a cluster. The following two flights are analyzed in the same manner, and the process continues with more and more flights added to the cluster. A cluster is considered to have ended as soon as a pair of flights is found that – when added – do not continue the forward motion of the tracer by at least 3 vortex widths.

PDFs of cluster lengths are displayed in Fig. 5 as open squares. For $a/a_2 = 1.0$ (Fig. 5b), clustering of the smaller flights results in a reduction in the PDF at small lengths and an increase at intermediate lengths. The result is a smaller decay exponent for small lengths: $\mu_{cluster} = 1.7 \pm 0.3$ over this range. Considering the theoretical predictions in Eq. 2, this scaling is consistent with the almost-ballistic growth of the variance ($\gamma = 2$) seen as a transient in Fig. 4(b). Clustering is *not* significant for the very long flights, though, and the two PDFs match up at the larger lengths.

Correlations are not as significant for $a/a_2 = 5.0$. There *is* a slightly increased probability that a flight will be followed by another flight in the opposite direction. The following flight, however, has an equivalent average magnitude in the direction of the original flight, so the pair adds up – on the average – to zero. The open squares in Fig. 5(a) show the PDF of cluster lengths for $a/a_2 = 5.0$. This PDF has almost exactly the same statistics as for individual flights; consequently, clustering does not play a significant role in this case.

The implication here is that the statistics of the flights alone are not sufficient to determine the long-range transport behavior if the flights have significant correlations. An analysis based on flight clusters gives a better prediction of the scaling behavior of the variance of a distribution.

There is another important deviation between the models used in the theoretical predictions (Eq. 2) and the current system. Whereas the theories [6] assume constant velocity flights, in this system different flights have different velocities. This fact is revealed in scatter plots of flight length versus speed, as is shown in Fig. 6(b). [7] A few dominant speeds are apparent for the shorter length flights, each speed corresponding to sticking of trajectories to a different island in the Poincaré sections of Fig. 3. Fewer of the islands are able to maintain the longer flights, however, evidenced by the dropping out of some of the velocities as the flight length increases. As seen in Fig. 6(b), flights with lengths greater than 50 vortex widths are dominated by a single flight velocity. The implication of these results is that each island may be associated with its own PDF for sticking and that, in general, characterization of the flights with a single flight length PDF may result in an incomplete description of the phenomena. The success of the theories [6] in predicting the long-time behavior for this system stems from the fact that the long flights are dominated by a single velocity.

Experiments are currently in progress to test these results. In the experiments, the horizontal chain of vortices is producd by a magnetohydrodynamic technique, [8] while the vertical vortices are generated by thermal convection from heating and cooling strips. Preliminary results show trajectories that are qualitatively similar to those from the simulations. More data is needed to make quantitative comparisons, though. This will be the subject of a future article.

We are pleased to acknowledge discussions with I. Mezic, J. Klafter and M. Shlesinger. These studies are supported by NSF grants PHY-9732158 and DMR-0071771. Equipment used in these studies was funded by a Cottrell College Science Award of Research Corporation.

---

* Electronic mail: tsolomon@bucknell.edu
† Current address: Department of Mechanical and Aerospace Engineering, Cornell University. Electronic mail: fogleman@mae.cornell.edu

[1] H. Aref, J. Fluid Mech. **143**, 1 (1984); J.M. Ottino, *The Kinematics of Mixing: Stretching, Chaos, and Transport* (Cambridge University Press, Cambridge, 1989).
[2] V.I. Arnold, C. R. Acad. Sci. Paris **261**, 17 (1965).
[3] A. N. Yannacopoulos, I. Mezic, G. Rowlands, and G. P. King, Phys. Rev. E **57**, 482 (1998).
[4] E.W. Montroll and M.F. Shlesinger, in *Nonequilibrium Phenomena II: From Stochastics to Hydrodynamics*, Studies in Statistical Mechanics Vol. II, edited by J. L. Lebowitz and E.W. Montroll (North-Holland, Amsterdam, 1984), p. 1; M.F. Shlesinger, G.M. Zaslavsky, and J. Klafter, Nature **363**, 31 (1993); T.H. Solomon, E.R. Weeks, and H.L. Swinney, Phys. Rev. Lett. **71**, 3975 (1993).
[5] M. Ding, T. Bountis, and E. Ott, Phys. Lett. A **151**, 395 (1990); Y.-C. Lai, M. Ding, C. Grebogi, and R. Blümel, Phys. Rev. A **46**, 4661 (1992); G.M. Zaslavsky, D. Stevens, and H. Weitzner, Phys. Rev. E **48**, 1683 (1993).
[6] J. Klafter, A. Blumen, and M.F. Shlesinger, Phys. Rev. A **35**, 3081 (1987); X.-J. Wang, Phys. Rev. A **45**, 8407 (1992); M.F. Shlesinger, J. Stat. Phys. **10**, 421 (1974); J. Klafter and G. Zumofen, Phys. Rev. E **49**, 4873 (1994); E.R. Weeks and H.L. Swinney, Phys. Rev. E **57**, 4915 (1998).
[7] L. Kuznetsov and G.M. Zaslavsky, Phys. Rev. E **61**, 3777 (2000).
[8] H. Willaime, O. Cardoso, and P. Tabeling, Phys. Rev. E **48**, 288 (1993); T.H. Solomon, S. Tomas, and J.L. Warner, Phys. Rev. Lett. **77**, 2682 (1996).